

Journal of Materials Chemistry A

Materials for energy and sustainability

Accepted Manuscript

This article can be cited before page numbers have been issued, to do this please use: Z. Li, J. Zhang, X. Jing, J. Dong, H. Liu, H. Lv, Y. Chi and C. Hu, *J. Mater. Chem. A*, 2020, DOI: 10.1039/D0TA09421H.



This is an Accepted Manuscript, which has been through the Royal Society of Chemistry peer review process and has been accepted for publication.

Accepted Manuscripts are published online shortly after acceptance, before technical editing, formatting and proof reading. Using this free service, authors can make their results available to the community, in citable form, before we publish the edited article. We will replace this Accepted Manuscript with the edited and formatted Advance Article as soon as it is available.

You can find more information about Accepted Manuscripts in the [Information for Authors](#).

Please note that technical editing may introduce minor changes to the text and/or graphics, which may alter content. The journal's standard [Terms & Conditions](#) and the [Ethical guidelines](#) still apply. In no event shall the Royal Society of Chemistry be held responsible for any errors or omissions in this Accepted Manuscript or any consequences arising from the use of any information it contains.

ARTICLE

Polyoxometalate@covalent triazine framework as robust electrocatalyst for selective benzyl alcohol oxidation coupled hydrogen productionReceived 00th January 20xx,
Accepted 00th January 20xx

DOI: 10.1039/x0xx00000x

Zhen Li, Junhao Zhang, Xiaoting Jing, Jing Dong, Huifang Liu, Hongjin Lv,* Yingnan Chi* and Changwen Hu

Electrocatalytic oxidation has been proven as a sustainable and promising alternative to traditional chemical transformation, but its further development is limited by the use of noble-metal electrocatalysts. Herein, a polyoxometalate-based electrode material, $\text{H}_5\text{PMo}_{10}\text{V}_2\text{O}_{40}\text{@CTF}$ (denoted as $\text{PMo}_{10}\text{V}_2\text{@CTF}$), has been successfully fabricated through electrostatic assembly of molecular polyoxometalate catalyst, $\text{PMo}_{10}\text{V}_2$, with the porous cationic covalent triazine framework (CTF), which, to our knowledge, represents the first combination of polyoxometalate with cationic CTF. The resulting $\text{PMo}_{10}\text{V}_2\text{@CTF}$ exhibits high activity for the selective electrocatalytic oxidation of alcohols to aldehydes, achieving 99% conversion of benzyl alcohol, over 99% selectivity of benzyl aldehyde, and at the same time near unity H_2 production. Notably, the reported electrocatalytic system presents good atom economy, high energy conversion (96% Faradaic efficiency), remarkable catalytic activity and robustness for at least eight recycles. Based on the various experimental and spectroscopic analyses, a possible catalytic mechanism was proposed, revealing that such excellent electrocatalytic performance is attributed to the versatile redox ability of $\text{PMo}_{10}\text{V}_2$ and the good porosity and adsorption property of CTF in the constructed $\text{PMo}_{10}\text{V}_2\text{@CTF}$ composite.

Introduction

Electrocatalytic organic synthesis has attracted increasing attention as a potential sustainable alternative to conventional chemical synthetic approach.¹⁻⁹ To date, important progress has been made on the anodic oxidations of alcohols, biomass-driven molecules, arenes, and aliphatic hydrocarbons,¹⁰⁻¹⁴ but most of these oxidation processes require the use of noble-metal-based electrocatalysts (such as Pt, Rh, Ru and Pd).¹⁵⁻¹⁹ To achieve economic and value-added transformation of organic substrates, some works have been reported on electrocatalytic oxidation of alcohols, in the meanwhile, coupling with hydrogen production. In these works, the organic substrates are electrocatalytically oxidized to fine chemicals on the anodic working electrode; while hydrogen as a clean and renewable energy is simultaneously released from cathodic counter electrode.^{3, 20-22} However, the challenges facing by these systems still remain in the following aspects. For example, electrooxidized carboxylic acid products (such as benzoic acid or 2,5-furandicarboxylic acid) were generally obtained and the selective oxidation of alcohols to corresponding aldehydes remains still a big challenge.^{23, 24} The high selectivity towards aldehydes in some systems requires the use of expensive

homogeneous 2,2,6,6-tetramethyl-1-piperidine-N-oxyl (TEMPO) as an electrocatalyst or co-catalyst, rendering this approach less attractive.^{10, 20, 25-30} Therefore, the development of facile catalytic systems using earth-abundant and effective catalyst under mild conditions is of scientific significance.

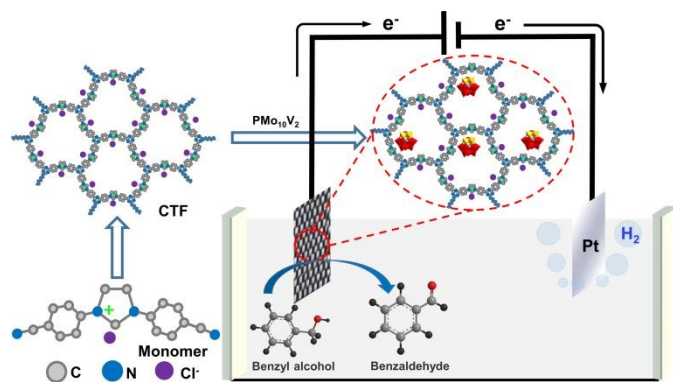
As an emerging type of catalysts, polyoxometalates (POMs) have been attracting tremendous attention due to their atomically well-defined structures and unique acid-base and redox properties.³¹⁻³⁵ POMs as a kind of promising molecular electrocatalysts can undergo fast and reversible stepwise electron transfer usually coupling with proton transfer.³⁶ For example, Neumann et al. explored the electrochemical hydroxylation of arenes catalyzed by homogeneous $[\text{Co}^{\text{III}}\text{W}_{12}\text{O}_{40}]^{5-}$ catalyst; Hill et al reported the tetra Ru-containing POMs for the effectively electrocatalytic oxidation of ethanol and methanol.^{37, 38} Nevertheless, the direct use of POMs as electrode materials are limited due to their poor attachment onto the electrode surface, low surface area, and poor electrical conductivity. To overcome these disadvantages, carbon-based materials and metal organic frameworks were largely developed to immobilize POMs. And these previous investigations reveal that nature of supports and immobilization strategy have significant influence on the stability and electrocatalytic activity of POMs.^{34, 39-42}

Covalent triazine frameworks (CTFs) are crosslinked porous polymers based on aromatic triazine units, which provide a promising platform for the immobilization of electrocatalysts owing to their large surface area, excellent chemical stability, good conductivity, and unique structure flexibility.⁴³⁻⁴⁵ To date, some active metal centers (such as Ru, Pt, Cu, and Pd etc.) have

Key Laboratory of Cluster Science Ministry of Education, Beijing Key Laboratory of Photoelectro/Electrophotonic Conversion Materials, School of Chemistry and Chemical Engineering, Beijing Institute of Technology, Beijing, 100081, People's Republic of China. E-mail: chiyingnan7887@bit.edu.cn; hlv@bit.edu.cn

*Electronic Supplementary Information (ESI) available: [proposed mechanism process for the selective electrocatalytic oxidation of BA coupled with H_2 evolution]. See DOI: 10.1039/x0xx00000x

been combined with CTFs and the resulting metal-modified CTFs exhibited remarkable activities in the electrochemical oxygen reduction reaction.⁴⁶⁻⁵¹ However, the combination of POM catalysts with CTFs are rarely reported.⁵² Herein, a novel electrocatalytic material, **PMo₁₀V₂@CTF**, has been successfully fabricated by using cationic CTF as support, where the active anionic Keggin-type clusters are evenly dispersed on the CTF and immobilized onto the support through electrostatic interactions. The synthesized **PMo₁₀V₂@CTF** as a noble metal free anode can effectively catalyze the selective oxidation of benzyl alcohol to benzaldehyde coupled with simultaneous H₂ production (Scheme 1), achieving high Faradaic efficiency (96%) and selectivity (>99%).



Scheme 1. Schematic of **PMo₁₀V₂@CTF** fabrication and **PMo₁₀V₂@CTF** as electrocatalyst for selective oxidation of benzyl alcohol coupled H₂ production.

Results and discussion

The cationic CTFs were synthesized through the trimerization of 1,3-bis(4-cyanophenyl)imidazolium chloride in molten ZnCl₂ (Scheme 1).⁵³ As shown in Fig. 1, comparing with FT-IR spectrum of monomer, the disappearance of characteristic C≡N stretching band at 2228 cm⁻¹ indicates the complete transformation of nitrile group to triazine, while the broad peaks at 1500-1616 cm⁻¹ and 1384-1463 cm⁻¹ reveal the presence of triazine and imidazole groups. Moreover, the formation of triazine rings was further confirmed by solid-state ¹³C cross-polarization magic-angle spinning nuclear magnetic resonance (¹³C CP/MAS NMR) spectrum (Fig. S2), where the peaks at 176 ppm and 129 ppm can be assigned to triazine carbon atoms and the phenyl group, respectively. For ionothermal method conducted at high temperature (500 °C), irreversible carbonization reactions occur in the synthesis of CTF, which could improve the conductivity of CTF due to the partial graphitization. As a result, the molar ratio of N to C (0.09) in CTF is far less than the theoretical value (0.27).

Considering the outstanding oxidizing activity of Keggin-type H₅PMo₁₀V₂O₄₀ (**PMo₁₀V₂**) for mediating electron transfer, it was chosen as the catalytic active species to combine with cationic CTFs. As shown in Scheme 1 and Fig. S3, when cationic CTFs were impregnated into the aqueous solution of **PMo₁₀V₂**, the color of **PMo₁₀V₂** gradually disappeared, revealing the successful ion exchange of POMs with Cl⁻. As shown in Fig. 1, all the characteristic peaks of **PMo₁₂V₂** can be clearly observed

from the FT-IR spectrum of **PMo₁₀V₂@CTF**, indicating the structural integrity of **PMo₁₀V₂** after immobilization. Compared with bare **PMo₁₀V₂**, the vibrations at 1049 cm⁻¹ for P-O_a (a: tetrahedral oxygen atoms), 945 cm⁻¹ for M=O_d (d: terminal oxygen atoms), and 877 cm⁻¹ for M-O_b-M (b: corner shared oxygen atoms) are nearly unchanged, but a slight blue shift of M-O_c-M (c: edge-shared oxygen atoms) from 771 to 786 cm⁻¹ is found, which is probably caused by the strong electrostatic interaction between POMs and CTF. According to the structural feature of CTF, we speculate that **PMo₁₀V₂** could be anchored around the imidazolium group. According to inductively coupled plasma atomic emission spectrometry (ICP-AES), the maximum loading amount of **PMo₁₀V₂** is calculated to be 28 wt% and the molar ratio of Mo to V is 4.8:1, which is close to the theoretical ratio of 5:1.

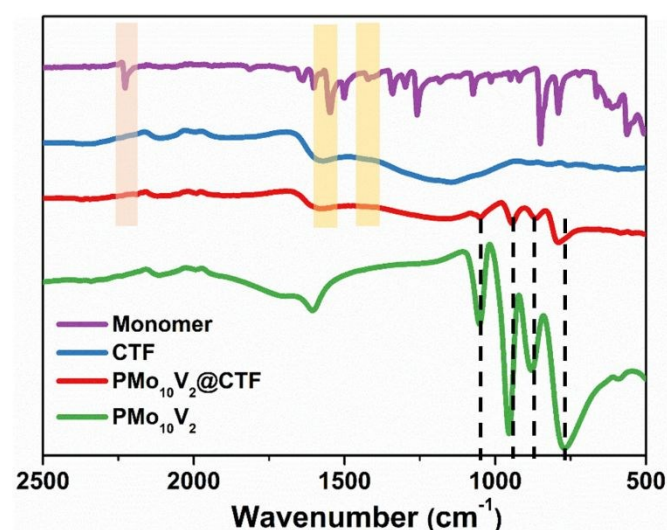


Fig. 1. FT-IR spectra of monomer, CTF, **PMo₁₀V₂@CTF**, and **PMo₁₀V₂**.

The observation of a broad peak in powder X-ray diffraction (PXRD) pattern suggests that **PMo₁₀V₂@CTF** is amorphous (Fig. S4) and there is no characteristic diffraction of POMs, displaying that **PMo₁₀V₂** are evenly dispersed on the CTF support. The Raman spectra of CTFs and **PMo₁₀V₂@CTF** (Fig. S5) show a G band at 1584 cm⁻¹ and a D band at 1341 cm⁻¹, which are attributed to sp²-hybridized carbon and disordered sp³ carbon, respectively. Interestingly, the value of I_D / I_G ratio increases after the incorporation of POMs, reflecting the increase of defects and disorders in **PMo₁₀V₂@CTF**.

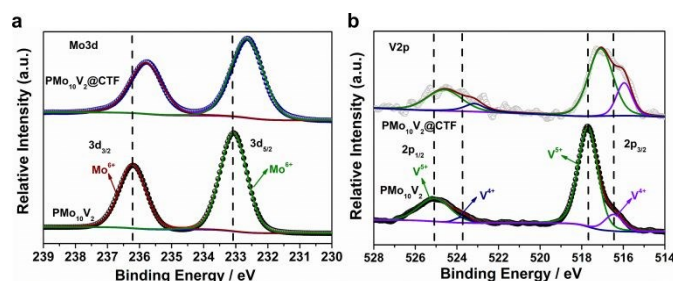


Fig. 2. XPS spectra (a) Mo 3d and (b) V 2p of **PMo₁₀V₂** and **PMo₁₀V₂@CTF**.

To confirm the elemental composition and their chemical oxidation state, X-ray photoelectron spectroscopy (XPS)

measurements were performed on both **PMo₁₀V₂@CTF** and **PMo₁₀V₂** samples (Fig. 2, Fig. S6-S9). The P 2p, Mo 3d, and V 2p signals are clearly detected in the XPS spectra of **PMo₁₀V₂**. The peaks with the binding energies of 236.2 eV (Mo 3d_{3/2}) and 233.05 eV (Mo 3d_{5/2}) confirm the +6 oxidation state of Mo atoms. In the V 2p region, two peaks at 525.1 eV and 517.7 eV are assigned to V 2p_{1/2} and V 2p_{3/2}, respectively, consistent with V⁵⁺ oxidation state, another two peaks at 523.7 eV (V 2p_{1/2}) and 516.45 eV (V 2p_{3/2}) are assigned to V⁴⁺ oxidation state, respectively (Fig. 2b). Notably, after immobilization the binding energy of Mo 3d (235.8 and 232.65 eV are assigned to Mo 3d_{3/2} and Mo 3d_{5/2}, respectively) in the **PMo₁₀V₂@CTF** composite shifts to lower region, meanwhile the ratio of V⁴⁺ (523.2 and 515.95 eV are assigned to V 2p_{1/2} and V 2p_{3/2}) species in the composite also obviously increases,⁴² and the binding energy of V 2p (**PMo₁₀V₂@CTF**) shifts to lower region about 0.5 eV, indicating partial electron transfer from CTF to **PMo₁₀V₂** during the formation of **PMo₁₀V₂@CTF** composite. The observed electron transfer behavior and coexistence of V⁵⁺ and V⁴⁺ are proven to be helpful for the improvement of electrocatalytic activity. The existence of P in **PMo₁₀V₂@CTF** has been further proven by solid-state ³¹P NMR spectroscopy (Fig. S10), where the slight peak shift relative to **PMo₁₀V₂** was found, probably due to the chemical environment change around P after combination with CTF. In addition, the strong interaction between **PMo₁₀V₂** and CTF support is further confirmed by leaching test. After soaking **PMo₁₀V₂@CTF** composite in water/acetonitrile for 8 h, no characteristic absorption of POMs was detected by UV-vis spectroscopy (Fig. S11).

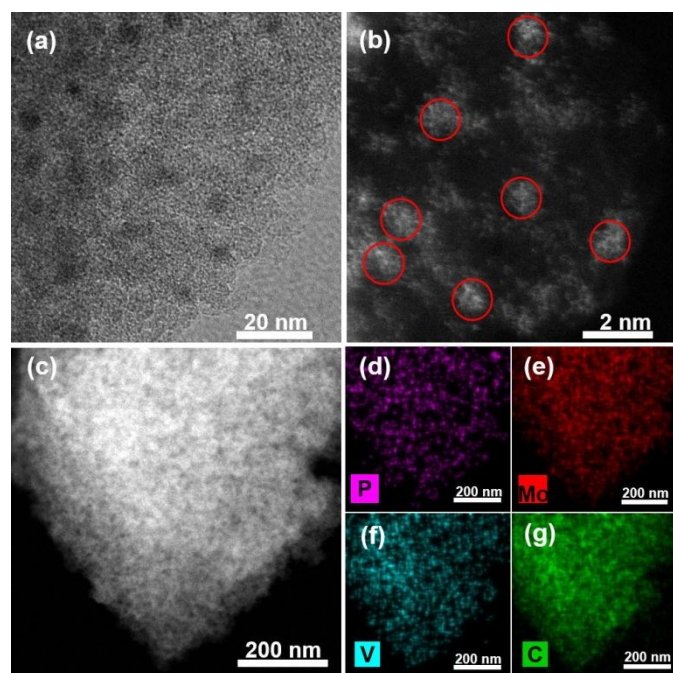


Fig. 3. (a) HRTEM image; (b) HAADF-STEM; (c)-(g) EDX elemental mapping of **PMo₁₀V₂@CTF**.

Moreover, the structure of **PMo₁₀V₂@CTF** composite is characterized by high-resolution transmission electron microscopy (HRTEM). As shown in Fig. 3a, there is no lattice

fringe in the HRTEM image due to its amorphous structure and POMs clusters (the black spots) are homogeneously dispersed in the support. By using high-angle annular dark-field scanning transmission electron microscopy (HAADF-STEM), bright spots corresponding to single **PMo₁₀V₂** cluster of about 1 nm and double clusters of about 2 nm can be clearly observed (Fig. 3b). Energy-dispersive X-ray (EDX) elemental mapping analysis of **PMo₁₀V₂@CTF** (Fig. 3c-3g) further reveals that Mo, V, P, and C atoms are uniformly distributed in the framework of CTF.^{54, 55} We speculate that the uniform distribution of POMs is possibly related to the special structure of cationic CTF. The synthesized **PMo₁₀V₂@CTF** with mesoporous structure and evenly dispersed **PMo₁₀V₂** is expected to be a promising electrode material for selective oxidation of alcohols as proved in the following experiments.

N₂ adsorption and desorption isotherms of CTF and **PMo₁₀V₂@CTF** are present in Fig. S13. Cationic CTF exhibits a type IV isotherm with a significant hysteresis loop in the range of $0.6 < p/p_0 < 0.9$, suggesting a mesoporous structure. However, the shape of curve is changed after loading POMs. **PMo₁₀V₂@CTF** has a Brunauer–Emmett–Teller (BET) surface area of 399 m² g⁻¹, which is much lower than that of CTF (1154 m² g⁻¹). Notably, the surface area of **PMo₁₀V₂@CTF** is much larger than many reported POMs-containing porous materials (Table S1). The pore size distribution of CTF (Fig. S14 and Table S2) contains both micropores of 1.7 nm and mesopores of 4-35 nm. After incorporation of Keggin-type POMs (~1.2 nm size), the pores of 1.7 nm disappear and the distribution range of mesopores (4-20 nm) becomes narrower relative to that of CTF (4-35 nm). The decrease of specific surface area and pore size (Table S2) shows that **PMo₁₀V₂** cluster is successfully incorporated into the pores of CTF.

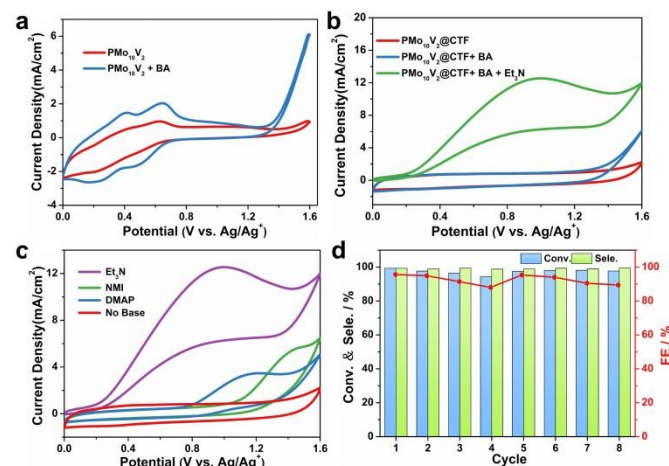


Fig. 4. (a) CVs of 1 mM **PMo₁₀V₂** in acetonitrile containing LiClO₄ (1.5 mmol) without benzyl alcohol (BA) and with 0.6 mmol BA, obtained at carbon cloth working electrode with a scan rate of 50 mV s⁻¹; (b) CVs of **PMo₁₀V₂@CTF** without BA, or with 0.6 mmol BA, or with 0.6 mmol BA and 0.18 mmol Et₃N, obtained at carbon cloth working electrode modified with **PMo₁₀V₂@CTF** (0.3 mg/cm²) with a scan rate of 50 mV s⁻¹ using LiClO₄ (1.5 mmol) as electrolyte; (c) CVs of **PMo₁₀V₂@CTF** upon addition of three different Brønsted bases (0.18 mmol) and BA (0.6 mmol), LiClO₄ (1.5 mmol), obtained at carbon cloth working electrode modified with **PMo₁₀V₂@CTF** (0.3

mg/cm²) with a scan rate of 50 mV s⁻¹; (d) Recycle test for the selective electrocatalytic oxidation of BA using **PMo₁₀V₂@CTF**.

The electrocatalytic activities of **PMo₁₀V₂@CTF** was initially evaluated by cyclic voltammetry method. Fig. 4a presents the cyclic voltammograms (CV) of 1 mM **PMo₁₀V₂** acetonitrile solution in the absence or presence of benzyl alcohol (BA). Upon addition of BA, a significant increase in the anodic peak current was observed, reflecting that quick catalytic response of **PMo₁₀V₂** towards the electrochemical oxidation of BA. Then the CV studies were performed using **PMo₁₀V₂@CTF**-modified carbon cloth electrode (Fig. 4b). Similar to that observed in **PMo₁₀V₂** solution, the addition of BA results in an increase in catalytic current. To further confirm the catalytic role of **PMo₁₀V₂** in the oxidation of BA, the CV curves of CTF without BA and with BA were recorded. Different from **PMo₁₀V₂** and **PMo₁₀V₂@CTF**, the addition of BA leads to a negligible increase in the anodic peak current (Fig. S15). Notably, the above-mentioned anodic current is further improved by addition of triethylamine (Et₃N) (Fig. 4b), which is consistent with previous literature report that Brønsted bases could enhance the electrocatalytic oxidation of alcohols. As shown in Fig. 4c, the addition of different organic bases (N-methylimidazole (NMI), 4-(dimethylamino)pyridine (DMAP), and Et₃N) could all promote the oxidation of BA, among which Et₃N base is particularly effective.

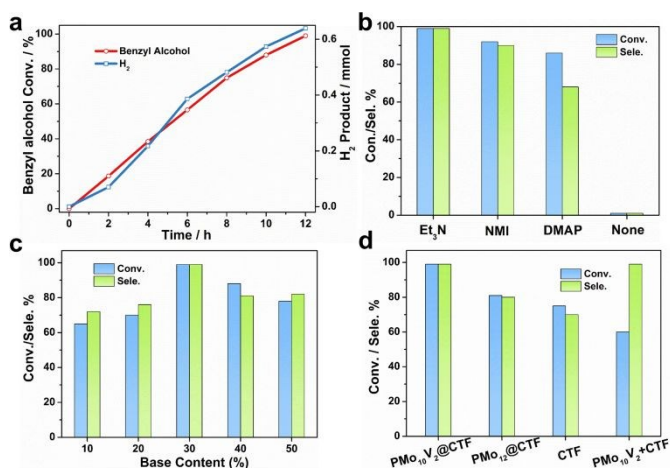


Fig. 5. (a) Time profile for the electrocatalytic oxidation of BA and simultaneous H₂ production using **PMo₁₀V₂@CTF** as anode; (b) The influence of different organic bases on the selective electrocatalytic oxidation of BA catalyzed by **PMo₁₀V₂@CTF**; (c) The influence of Et₃N amount on the selective electrocatalytic oxidation of BA catalyzed by **PMo₁₀V₂@CTF**; (d) Selective electrocatalytic oxidation of BA using different catalysts. Reaction conditions: BA (0.6 mmol), anhydrous acetonitrile (10 mL), Et₃N (0.18 mmol), and LiClO₄ (1.5 mmol) at ambient conditions for 12 h with the potential of 1.6 V vs. Ag/Ag⁺.

Bulk electrolysis experiment of BA was performed in an electrolysis cell using **PMo₁₀V₂@CTF**-modified carbon cloth (1.0 cm²) as working electrode, platinum foil as counter electrode, and Ag/Ag⁺ electrode as reference electrode, respectively. The acetonitrile solution containing BA, Et₃N (30 mol% relative to BA), and LiClO₄ electrolyte was added to the cell and a potential

of 1.6 V (vs. Ag/Ag⁺ reference electrode) was applied. As shown in Fig. 5a, the conversion of BA linearly increases with electrolysis time and 99% of BA is converted in 12 h under ambient conditions. More importantly, no undesired over-oxidation product (benzoic acid) was detected by gas chromatography (GC) (Fig. S16) and the selectivity for benzaldehyde reaches over 99%, corresponding to a Faradaic efficiency (FE) of 96%. The FE of hydrogen production is 98%. During the electrolysis process, a large amount of hydrogen gas was generated over time at the cathode part (as shown in the supporting Video clip). Moreover, the H₂ evolution rate is proportional to the conversion rate of substrate. After 12 h, ~0.639 mmol H₂ was measured by GC. Recently, nitrogen-doped carbon@CuCo₂N_x (NC@CuCo)²¹ and nickel hydroxide nanosheets, h-Ni(OH)₂⁵⁶, have been proven to be active for the selective electrocatalytic oxidation of alcohols to aldehydes with simultaneous H₂ production, but in their experiments TEMPO was used to improve the selectivity for benzaldehydes. The catalytic performance of **PMo₁₀V₂@CTF** (conversion: 99%, selectivity: >99%, FE: 96%) reported in our work outperforms that of NC@CuCo (conversion: 97%, selectivity: >98%, FE: 76%)²¹ and h-Ni(OH)₂ (conversion: >90%, selectivity: >94%, FE: 81.3%)⁵⁶ (Table S3).

In addition, we find that organic bases play a crucial role in the electrocatalytic reaction. As shown in Fig. 5b, a negligible amount of benzaldehyde is detected in the absence of organic base. In contrast, the addition of a small amount of organic bases (30 mol% relative to BA) greatly improved both conversion and selectivity. Under otherwise identical conditions, the catalytic performance of Et₃N (conversion: 99%, selectivity: >99%) is better than that of NMI (conversion: 89%, selectivity: 90%) and DMAP (conversion: 86%, selectivity: 79%). The order of Et₃N > NMI > DMAP in controlled potential electrolysis is consistent with the results of CV measurements (Fig. 4b). The influence of Et₃N amount on electrocatalytic activity was also studied. As shown in Fig. 5c, with the increase of Et₃N amount both conversion and selectivity show a first increasing and then decreasing trend, and the optimal amount of added organic base is 30%. As POMs are sensitive to pH, the addition of more Et₃N (above 30%) would lead to the decomposition of **PMo₁₀V₂**, accordingly leading to the decreased catalytic activity. Based on above results, we speculate that in our system Et₃N probably works as the proton-transfer mediator: it accepts the proton at the anode to form Et₃NH⁺, which is subsequently reduced to H₂ and Et₃N at the cathode.

To assess the influence of POMs and CTF on the electrocatalytic activity, a series of control experiments were conducted under the otherwise identical conditions. As shown in Fig. 5d, 72% of BA was converted by CTF electrode, showing CTF support is active for the electrochemical oxidation of BA, but the selectivity for benzaldehyde (65%) is unsatisfactory. After incorporation of **PMo₁₀V₂**, both the conversion and selectivity were significantly improved. When **PMo₁₂@CTF** (**PMo₁₂**: H₃PMo₁₂O₄₀, the other Keggin-type cluster) was used as electrocatalyst, an obvious decrease in catalytic performance was found (Fig. 5d). Such different catalytic performances of

PMo₁₀V₂@CTF (conversion: 99%, selectivity: >99%) and **PMo₁₂@CTF** (conversion: 79%, selectivity: >69%) indicates the important contribution of substituted V atoms in **PMo₁₀V₂** (Fig. 5d). The electrochemical oxidation of BA with homogeneous **PMo₁₀V₂** using CTF-modified carbon cloth as electrode was also tested (Fig. 5d). The addition of **PMo₁₀V₂** yields a high selectivity (>99%) of the electrocatalytic oxidation reaction showing the important role of **PMo₁₀V₂**, but the conversion (60%) of BA in the presence of homogeneous **PMo₁₀V₂** is much lower than that of **PMo₁₀V₂@CTF** composite. During the electrocatalytic reaction using **PMo₁₀V₂** as homogeneous catalyst, the reaction solution gradually changed from yellow to green, indicating that **PMo₁₀V₂** was reduced. However, the re-oxidation of reduced-**PMo₁₀V₂** only occurs when it diffuses to the surface of anode, which hinders the turnover of homogeneous POM in some degree. When **PMo₁₀V₂** is immobilized on CTF to fabricate electrode material, electron transfer between **PMo₁₀V₂** and electrode can go smoothly, leading to its remarkable performance.

For electrocatalytic materials, their recyclability and stability are key issues for potential practical applications. As shown in Fig. 4d, the **PMo₁₀V₂@CTF** catalyst is highly recyclable and even after 8 consecutive cycles the conversion of BA remained above 98% and a FE of 90% was achieved. Impressively, during the recycle process no over-oxidation product (e.g. benzoic acid) was detected. To confirm the stability of **PMo₁₀V₂@CTF** composite in the presence of Et₃N, the composite was soaked in the reaction solution for 7 days and FT-IR spectrum of isolated samples remains unchanged (Fig. S17). In addition, after the electrocatalytic reaction the catalyst on electrode and reaction solution were collected. For the post-reaction solution, no characteristic absorption of **PMo₁₀V₂** is detected by UV-vis spectrum (Fig. S18), while for the catalyst there is no obvious change found in the FT-IR spectra before and after the electrocatalysis (Fig. S19). The XPS spectrum of the recycled catalyst was also measured, where the V 2p (Fig. 6a) and Mo 3d (Fig. 6b) peaks are basically unchanged relative to the pristine sample. Interestingly, the ratio of V⁴⁺ oxidation state increases in **PMo₁₀V₂@CTF** after the electrocatalytic reaction. Furthermore, the Mo 3d peaks could be deconvoluted into 235.8 eV (3d_{3/2}, Mo⁶⁺), 233.8 eV (3d_{3/2}, Mo⁵⁺), 232.65 eV (3d_{5/2}, Mo⁶⁺), and 232.05 eV (3d_{5/2}, Mo⁵⁺). Moreover, the V 2p peaks could be deconvoluted into 524.6 eV (2p_{1/2}, V⁵⁺), 517.1 eV (2p_{3/2}, V⁵⁺), 523.2 eV (2p_{1/2}, V⁴⁺), and 515.95 eV (2p_{3/2}, V⁴⁺), respectively. The presence of Mo⁵⁺ and the increase of V⁴⁺ imply that **PMo₁₀V₂@CTF** could accept the electrons by oxidizing BA substrate during the electrocatalytic reaction. Though, with some oxidation state variation, the structure and catalytic performance of **PMo₁₀V₂@CTF** are basically maintained for eight successive recycling test.

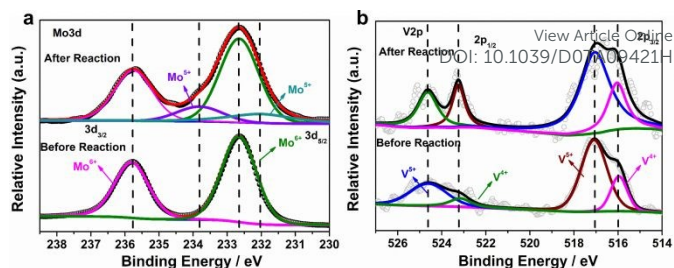


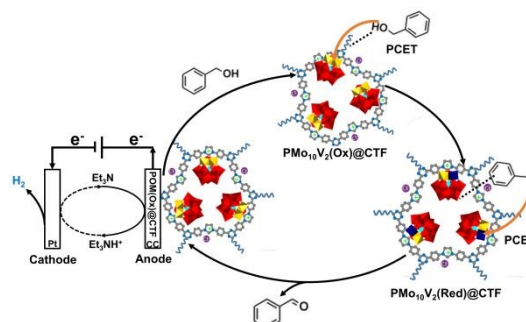
Fig. 6. XPS spectra of **PMo₁₀V₂@CTF** (a) Mo 3d and (b) V 2p of before and after the reaction.

The excellent electrocatalytic activity, stability, and recyclability of **PMo₁₀V₂@CTF** in the selective oxidation of BA prompted us to assess its performance in the oxidation of other benzylic alcohols (Fig. S20). Without any further optimization, **PMo₁₀V₂@CTF** is active for the electrochemical oxidation of benzylic alcohols to the corresponding aldehydes with the conversion of 91-99% and selectivity of 91-99% (Table 1, entries 1-5). It is noteworthy that the remarkable selectivity (>99%) was obtained for the benzylic alcohols with electron donating groups. In most cases, FE is higher than 80%. Although 90% of diphenylmethanol was converted, the reaction only gave a selectivity of 50% for diphenyl ketone due to the formation of by-product tetraphenylethylene (Table 1, entry 6).

Table 1. Electrochemical oxidation of alcohols using **PMo₁₀V₂@CTF**^a

Entry	Substrate	Product	Conv. ^b	Sele. ^b	FE (%)
1			99	99	96
2			93	99	87
3			95	99	83
4			99	91	95
5			91	95	85
6			90	50	77

^a Reaction conditions: alcohols (0.6 mmol), anhydrous acetonitrile (10 mL), Et₃N (0.18 mmol), LiClO₄ (1.5 mmol), reaction time: 12 h, E: 1.6 V vs. Ag/Ag⁺. ^b The product conversion and selectivity were determined by GC analysis.



Scheme 2. Proposed mechanism for the selective electrocatalytic oxidation of benzyl alcohol by **PMo₁₀V₂@CTF**.

We also conducted the adsorption test of BA on **PMo₁₀V₂@CTF** and quantified the amount of adsorbed BA by GC. Since **PMo₁₀V₂@CTF** has relative higher specific surface area and well-defined mesoporous structure, it exhibits substrate adsorption capacity towards BA and the maximum adsorbed amount is about 28 mmol/g (Fig. S21). We speculate that BA possibly interacts with CTF by hydrogen bonding between the hydroxyl group of BA and nitrogen sites of CTF. According to previous investigations, we guess that a radical process might be involved in the electrochemical reaction. To verify our speculation, Ph₂NH as oxygen radical scavenger and tert-butanol as a hydroxyl radical scavenger were added into the reaction system. As shown in Table S4, the oxidation of BA was effectively prohibited by the addition of Ph₂NH. On the basis of above experimental results and XPS analysis, we propose a plausible mechanism for the selective electrocatalytic oxidation of BA coupled with H₂ evolution (Scheme 2). In the first stage, BA is adsorbed by CTF that is readily accessible to the immobilized POMs cluster. Then, the oxidized state of **PMo₁₀V₂(ox)@CTF** catalyzes BA to benzyl aldehyde through proton coupled electron transfer (PCET), generating the reduced state of **H₂PMo₁₀V₂(red)@CTF**. In addition, an oxygen radical species (PhCH₂O) might be involved in this step. The electron transfer from substrate to **PMo₁₀V₂** is partially supported by XPS data, where ratios of Mo⁵⁺ and V⁴⁺ increase after the electrocatalytic oxidation. In the meanwhile, the protons are removed from **H₂PMo₁₀V₂(red)@CTF** by Et₃N forming Et₃NH⁺ and the catalyst is oxidized to **PMo₁₀V₂(ox)@CTF** at anode completing a catalytic cycle. The mesoporous structure of CTF and electrostatic interactions between POMs and the CTF support facilitate the electron and proton transfer. In the cathodic electrode, Et₃NH⁺ is reduced to release H₂ and regenerate Et₃N at the same time.

Conclusions

In summary, we demonstrate a facile and effective strategy to fabricate POMs electrode material through electrostatic assembly of active **PMo₁₀V₂** cluster with cationic CTF support. The synthesized **PMo₁₀V₂@CTF** works as effective electrocatalyst for the selective oxidation of BA coupling with H₂ generation with near unity yield. The selectivity (>99%) and FE (96%) of **PMo₁₀V₂@CTF** is higher than those of the reported heterogeneous catalysts. Moreover, the catalyst is highly robust and recyclable and its catalytic activity is maintained even after eight successive cycles. Such catalytic system is also applicable to a variety of BA derivatives with very high conversion and selectivity. The exhibited electrocatalytic performance is mainly attributed to the versatile redox ability of **PMo₁₀V₂**, the porous architecture, highly dispersed POMs, and the cooperative effect between CTF and POMs. The reported investigations have important implications for the development of POMs-based electrocatalytic materials and also provides some insightful guidelines for oxidation of other organic substrates beyond alcohol oxidation.

Experimental

Materials and Methods.

All the starting materials and organic solvents were purchased from commercial suppliers and used without further purification unless otherwise noted. H₅PMo₁₀V₂O₄₀·nH₂O⁵⁷ and 1,3-bis(4-cyanophenyl)imidazolium chloride⁵⁸ were prepared according to literature methods. Solid-state ¹³C and ³¹P CP/MAS spectroscopy of **PMo₁₀V₂@CTF** and **PMo₁₀V₂** were performed at room temperature on a 700 MHz Bruker Ascend spectrometer at a MAS rate of 5 kHz. PXRD measurements were carried out on the Rigaku SmartLab X-ray diffractometer with Cu-Kα radiation (40 kV, 30 mA, λ = 1.5418 Å) and a scanning step of 0.01°. The morphology and microstructure of the samples were observed by scanning electron microscopy (SEM, JOEL JSE-7500F) and transmission electron microscopy (TEM, JOEL JEM-2010). The atomic resolution scanning transition electron microscopy (STEM) and energy-dispersive spectroscopy (EDS) experiments were performed on an aberration-corrected transmission electron microscope FEI Titan Cubed Themis G2 300. The FT-IR spectra were collected on a Nicolet 170SXFT-IR spectrophotometer in the range 400-4000 cm⁻¹. N₂ adsorption-desorption isotherms and pore size distribution were obtained at 77 K by using a Belsorp-max surface area detecting instrument. The XPS spectra of the samples were performed on Thermo ESCALAB 250Xi. The UV-vis spectra were measured on UV-2600. The Raman spectra were obtained on SNFT-SRLab1000. The inductively coupled plasma mass spectrometry (ICP-MS) were measured on Thermo Scientific iCAP Q. Gas chromatograph analyses were performed on a Shimadzu GC-2014C instrument with an FID detector equipped with an HP 5 ms capillary column. The quantity of hydrogen evolved was determined using a Techcomp GC-9700 gas chromatograph with a 5 Å molecular sieve column (2 m*2 mm) and a thermal conductivity detector (TCD). The thermogravimetric analysis (TGA) of the samples was performed using a Shimadzu DTG-60AH thermal analyzer under the N₂ atmosphere from room temperature to 800 °C with a heating rate of 5 °C min⁻¹. Elemental analyses (C, H and N) were performed on an ElementarVario EL cube Elmer CHN elemental analyzer.

Synthesis of CTF

The cationic CTF was synthesized according to the reported ionothermal method.⁵³ In a typical experiment, a mixture of 0.613 g (2 mmol) of 1,3-bis(4-cyanophenyl)imidazolium chloride and 1.363 g (10 mmol) of desiccated ZnCl₂ was placed into a quartz ampule under an inert atmosphere. The ampule was then evacuated, flame-sealed and transferred into a furnace for heating treatment at 500 °C for 40 h. The solid monolith obtained was subsequently grounded and then washed thoroughly with water to remove most of the ZnCl₂. Further stirring in 0.1 M HCl for 12 h was carried out to remove the residual salt. The resulting black powder was washed successively with water and THF and dried in vacuum at 120 °C

for 12 h. The C, H and N elemental analysis (%) for CTF: 66.09, 2.243, 6.031.

Synthesis of $\text{PMo}_{10}\text{V}_2\text{@CTF}$

$\text{PMo}_{10}\text{V}_2$ (0.05 g) was dissolved in deionized water (15 mL) and then CTF (100 mg) was added. The mixture was stirred at room temperature for 8 h and during the process the characteristic color of $\text{PMo}_{10}\text{V}_2$ gradually disappeared. Finally, a black solid of $\text{PMo}_{10}\text{V}_2\text{@CTF}$ was obtained after washing with a large amount of deionized water and drying at 80 °C for 12 h.

Electrochemical Oxidation of Benzyl Alcohols

Preparation of $\text{PMo}_{10}\text{V}_2\text{@CTF}$ electrode. The $\text{PMo}_{10}\text{V}_2\text{@CTF}$ working electrode was prepared as follows: $\text{PMo}_{10}\text{V}_2\text{@CTF}$ (5 mg) was dispersed in isopropanol (1 mL) containing 5 wt% Nafion under ultrasonic conditions. 50 μL of this suspension was drop-casted onto a piece of carbon cloth (1 cm^2) and then dried under vacuum.

Cyclic Voltammetry Experiments. Voltammetric experiments were performed in anhydrous acetonitrile (10 mL) containing supporting electrolyte LiClO_4 (1.5 mmol) at room temperature. All potentials were measured by a CH Instruments Electrochemical Analyzer (CHI660E) with a scan rate of 50 mV s^{-1} . The CV tests of homogeneous $\text{PMo}_{10}\text{V}_2$ (10mM) were performed using a three-electrode setup with glassy carbon (GC) working electrode (3 mm diameter), a platinum plate (1 cm^2) electrode as counter electrode and Ag/AgNO_3 as reference electrode. The CV tests of $\text{PMo}_{10}\text{V}_2\text{@CTF}$ were performed with $\text{PMo}_{10}\text{V}_2\text{@CTF}$ modified carbon cloth as working electrode (1 cm^2 effective area), a platinum foil as counter electrode and Ag/AgNO_3 electrode as reference electrode.

Controlled Potential Electrolysis Experiments. Bulk electrolysis experiments were performed in an undivided cell using a three-electrode setup with a $\text{PMo}_{10}\text{V}_2\text{@CTF}$ -modified carbon cloth (1.0 cm^2) as working electrode, a platinum foil as counter electrode, and a Ag/AgNO_3 electrode as reference electrode. To the cell was added 10 mL of anhydrous acetonitrile solution containing LiClO_4 (1.5 mmol), Et_3N (0.18mmol), and benzyl alcohol (0.6 mmol) and a potential of 1.6 V vs Ag/AgNO_3 was applied. At the end of electrolysis, biphenyl as internal standard was added in the reaction solution and the products were qualitatively analyzed by GC. For the recycle test, after the reaction the working electrode, $\text{PMo}_{10}\text{V}_2\text{@CTF}$ -modified carbon cloth, was gently washed with acetonitrile and ethyl alcohol for three times, dried and used for the next cycle.

Conflicts of interest

There are no conflict interest to declare.

Acknowledgements

This work was financially supported by the National Natural Science Foundation of China (21871025, 21831001, 21671019, 21871026, 21771020, and 21971010).

Notes and references

View Article Online

DOI: 10.1039/D0TA09421H

- W. Zhong, H. Liu, C. Bai, S. Liao and Y. Li, *ACS Catalysis*, 2015, **5**, 1850-1856.
- J. E. Nutting, M. Rafiee and S. S. Stahl, *Chem. Rev.*, 2018, **118**, 4834-4885.
- A. Das and S. S. Stahl, *Angew Chem Int Ed.*, 2017, **56**, 8892-8897.
- A. J. J. Lennox, J. E. Nutting and S. S. Stahl, *Chem Sci*, 2018, **9**, 356-361.
- Q. L. Yang, Y. Q. Li, C. Ma, P. Fang, X. J. Zhang and T. S. Mei, *J. Am. Chem. Soc.*, 2017, **139**, 3293-3298.
- C. Tian, L. Massignan, T. H. Meyer and L. Ackermann, *Angew Chem Int Ed.*, 2018, **57**, 2383-2387.
- C. Y. Cai and H. C. Xu, *Nat Commun*, 2018, **9**, 3551.
- B. Schille, N. O. Giltzau and R. Francke, *Angew Chem Int Ed.*, 2018, **57**, 422-426.
- D. T. Yang, M. Zhu, Z. J. Schiffer, K. Williams, X. Song, X. Liu and K. Manthiram, *ACS Catalysis*, 2019, **9**, 4699-4705.
- A. Badalyan and S. S. Stahl, *Nature*, 2016, **535**, 406-410.
- B. You, X. Liu, N. Jiang and Y. Sun, *J. Am. Chem. Soc.*, 2016, **138**, 13639-13646.
- E. J. Horn, B. R. Rosen, Y. Chen, J. Tang, K. Chen, M. D. Eastgate and P. S. Baran, *Nature*, 2016, **533**, 77-81.
- Y. Kawamata, M. Yan, Z. Liu, D. H. Bao, J. Chen, J. T. Starr and P. S. Baran, *J. Am. Chem. Soc.*, 2017, **139**, 7448-7451.
- J. A. Marko, A. Durgham, S. L. Bretz and W. Liu, *Chem Commun (Camb)*, 2019, **55**, 937-940.
- M. YASUZAWA, K. KAN, A. KIJUNGI, Z. OGUMI and Z. TAKEHARA, *Electrochim. Acta*, 1995, **40**, 1785-1787.
- A. L. B. Marques, W. Li, E. P. Marques and J. Zhang, *Electrochim. Acta*, 2004, **49**, 879-885.
- S. Yamazaki, M. Yao, N. Fujiwara, Z. Siroma, K. Yasuda and T. Ioroi, *Chem Commun*, 2012, **48**, 4353-4355.
- A. L. Wang, H. Xu, J. X. Feng, L. X. Ding, Y. X. Tong and G. R. Li, *J. Am. Chem. Soc.*, 2013, **135**, 10703-10709.
- Z. Daşdelen, Y. Yıldız, S. Eriş and F. Şen, *Appl. Catal., B*, 2017, **219**, 511-516.
- M. Rafiee, Z. M. Konz, M. D. Graaf, H. F. Koolman and S. S. Stahl, *ACS Catalysis*, 2018, **8**, 6738-6744.
- J. Zheng, X. Chen, X. Zhong, S. Li, T. Liu, G. Zhuang, X. Li, S. Deng, D. Mei and J.-G. Wang, *Adv. Funct. Mater.*, 2017, **27**, 1704169.
- X. Cui, M. Chen, R. Xiong, J. Sun, X. Liu and B. Geng, *J. Mater. Chem. A*, 2019, **7**, 16501-16507.
- N. Zhang, Y. Zou, L. Tao, W. Chen, L. Zhou, Z. Liu, B. Zhou, G. Huang, H. Lin and S. Wang, *Angew Chem Int Ed.*, 2019, **58**, 15895-15903.
- Z. Yin, Y. Zheng, H. Wang, J. Li, Q. Zhu, Y. Wang, N. Ma, G. Hu, B. He, A. Knop-Gericke, R. Schlogl and D. Ma, *ACS Nano*, 2017, **11**, 12365-12377.
- M. Rafiee, K. C. Miles and S. S. Stahl, *J. Am. Chem. Soc.*, 2015, **137**, 14751-14757.
- C. J. Weiss, E. S. Wiedner, J. A. Roberts and A. M. Appel, *Chem Commun*, 2015, **51**, 6172-6174.
- M. T. Masatoshi Shibuya, and Yoshiharu Iwabuchi, *J. Org. Chem.*, 2008, **73**, 4750-4752.
- B. L. Ryland and S. S. Stahl, *Angew Chem Int Ed.*, 2014, **53**, 8824-8838.
- M. H. A. Janssen, J. F. Chesa Castellana, H. Jackman, P. J. Dunn and R. A. Sheldon, *Green Chem.*, 2011, **13**, 905.

30. X. L. Renhua Liu, Chunyan Dong, and Xinquan Hu, *J. Am. Chem. Soc.*, 2004, **126**, 4112-4113.
31. J. Macht, M. J. Janik, M. Neurock and E. Iglesia, *Angew Chem Int Ed.*, 2007, **46**, 7864-7868.
32. I. A. Weinstock, R. E. Schreiber and R. Neumann, *Chem. Rev.*, 2018, **118**, 2680-2717.
33. E. D. Anne Dolbecq, Ce'dric R. Mayer, and Pierre Mialane, *Chem. Rev.*, 2010, **110**, 6009-6048.
34. F. M. Toma, A. Sartorel, M. Iurlo, M. Carraro, P. Parris, C. Maccato, S. Rapino, B. R. Gonzalez, H. Amenitsch, T. Da Ros, L. Casalis, A. Goldoni, M. Marcaccio, G. Scorrano, G. Scoles, F. Paolucci, M. Prato and M. Bonchio, *Nat Chem*, 2010, **2**, 826-831.
35. V. Y. Evtushok, A. N. Suboch, O. Y. Podyacheva, O. A. Stonkus, V. I. Zaikovskii, Y. A. Chesalov, L. S. Kibis and O. A. Kholdeeva, *ACS Catalysis*, 2018, **8**, 1297-1307.
36. Y. Ji, L. Huang, J. Hu, C. Streb and Y. F. Song, *Energy Environ. Sci.*, 2015, **8**, 776-789.
37. A. M. Khenkin, M. Somekh, R. Carmieli and R. Neumann, *Angew Chem Int Ed.*, 2018, **57**, 5403-5407.
38. Y. Liu, S. F. Zhao, S. X. Guo, A. M. Bond, J. Zhang, G. Zhu, C. L. Hill and Y. V. Geletii, *J. Am. Chem. Soc.*, 2016, **138**, 2617-2628.
39. C. Zou, Z. Zhang, X. Xu, Q. Gong, J. Li and C. D. Wu, *J. Am. Chem. Soc.*, 2012, **134**, 87-90.
40. S. Mukhopadhyay, J. Debgupta, C. Singh, A. Kar and S. K. Das, *Angew Chem Int Ed.*, 2018, **57**, 1918-1923.
41. H. Ma, B. Liu, B. Li, L. Zhang, Y. G. Li, H. Q. Tan, H. Y. Zang and G. Zhu, *J. Am. Chem. Soc.*, 2016, **138**, 5897-5903.
42. J. Song, Y. Li, P. Cao, X. Jing, M. Faheem, Y. Matsuo, Y. Zhu, Y. Tian, X. Wang and G. Zhu, *Adv. Mater.*, 2019, **31**, e1902444.
43. P. Kuhn, M. Antonietti and A. Thomas, *Angew Chem Int Ed.*, 2008, **47**, 3450-3453.
44. A. I. F. Pierre Kuhn, Dangsheng Su, Arne Thomas, and Markus Antonietti, *J Am Chem Soc*, 2008, **130**, 13333-13337.
45. X. Zhu, C. Tian, S. M. Mahurin, S. H. Chai, C. Wang, S. Brown, G. M. Veith, H. Luo, H. Liu and S. Dai, *J. Am. Chem. Soc.*, 2012, **134**, 10478-10484.
46. J. Artz, S. Mallmann and R. Palkovits, *ChemSusChem*, 2015, **8**, 672-679.
47. R. Palkovits, M. Antonietti, P. Kuhn, A. Thomas and F. Schuth, *Angew Chem Int Ed.*, 2009, **48**, 6909-6912.
48. K. Iwase, T. Yoshioka, S. Nakanishi, K. Hashimoto and K. Kamiya, *Angew. Chem. Int. Ed.*, 2015, **54**, 11068-11072.
49. Z. Wang, C. Liu, Y. Huang, Y. Hu and B. Zhang, *Chem Commun*, 2016, **52**, 2960-2963.
50. L. Zhao, S. Shi, G. Zhu, M. Liu, J. Gao and J. Xu, *Green Chem.*, 2019, **21**, 6707-6716.
51. M. Pilaski, J. Artz, H.-U. Islam, A. M. Beale and R. Palkovits, *Microporous Mesoporous Mater.*, 2016, **227**, 219-227.
52. S. Zhang, O. Oms, L. Hao, R. Liu, M. Wang, Y. Zhang, H. Y. He, A. Dolbecq, J. Marrot, B. Keita, L. Zhi, P. Mialane, B. Li and G. Zhang, *ACS Appl. Mater. Interfaces*, 2017, **9**, 38486-38498.
53. T.-T. Liu, R. Xu, J.-D. Yi, J. Liang, X.-S. Wang, P.-C. Shi, Y.-B. Huang and R. Cao, *ChemCatChem*, 2018, **10**, 2036-2040.
54. P. H. Qingda Liu, Hongde Yu, Lin Gu, Bing Ni, Dong Wang, Xun Wang, *Science Advances*, 2019, **5**, eaax1081.
55. J. Liu, W. Shi, B. Ni, Y. Yang, S. Li, J. Zhuang and X. Wang, *Nat Chem*, 2019, **11**, 839-845.
56. X. Chen, X. Zhong, B. Yuan, S. Li, Y. Gu, Q. Zhang, G. Zhuang, X. Li, S. Deng and J. G. Wang, *Green Chem.*, 2019, **21**, 578-588.
57. R. N. a. M. Lissel, *J. Org. Chem.*, 1989, **54**, 4607-4610.
58. R. S. Crees, M. L. Cole, L. R. Hanton and C. J. Sumby, *Inorg. Chem.*, 2010, **49**, 1712-1719.

Table of Contents

